A 10,000 yr record of high-resolution Paleosecular Variation from a flowstone of Rio Martino Cave, Northwestern Alps, Italy

Elena Zanella[1], Evdokia Tema[1], Luca Lanci[2], Eleonora Regattieri[3,4], Ilaria Isola[5], John C. Hellstrom[6], Emanuele Costa[1], Giovanni Zanchetta[5,7], Russell N. Drysdale[8,9], Federico Magrì[10]

[1]Dipartimento di Scienze della Terra, Via Valperga Caluso 35, 10125 Torino, Italy

[2]Dipartimento di Scienze Pure e Applicate, Piazza della Repubblica 13, 61029 Urbino, Italy

[3]Institute of Geology and Mineralogy, University of Cologne, Zülpicher Str. 49a, 50674 Cologne, Germany

[4]Istituto di Geoscienze e Georisorse IGG-CNR, via Moruzzi 1, 56100 Pisa, Italy

[5]Istituto Nazionale di Geofisica e Vulcanologia INGV, Via della Faggiola 32, 56126 Pisa, Italy

[6]School of Earth Sciences, University of Melbourne, Victoria 3010 Australia

[7]Dipartimento di Scienze della Terra, Via S. Maria 53 56126 Pisa, Italy

[8]School of Geography, University of Melbourne, Victoria 3010, Australia

[9]EDYTEM, UMR CNRS 5204, Université de Savoie-Mont Blanc, 73376 Le Bourget du Lac cedex, France

[10]Gruppo Speleologico Valli Pinerolesi GSVP, Club Alpino Italiano, Pinerolo, Italy

Abstract

Speleothems are potentially excellent archives of the Earth's magnetic field, suitable to record its past variations. Their characteristics, as the continuity of the record, the possibility to be easily dated, the almost instantaneous remanence acquisition and the high time-resolution make them potentially unique high-quality Paleosecular Variation (PSV) recorders. Nevertheless, speleothems are commonly characterized by low magnetic intensities and this often limits their resolution. Here we present a paleomagnetic study performed on two cores from a flowstone from the Rio Martino cave (Western Alps, Italy). Available U/Th dating indicates that the flowstone's deposition covers almost the Holocene, spanning the period ca. 0.5-9.0 ka, while an estimation of its mean growth rate is around 1 mm per 15 years. The flowstone is composed by columnar calcite, characterized by a high magnetic detrital content, arising from meta-ophiolites widely present in the cave's catchment, even if this detrital content did not compromised the quality of the U/Th dating and final age model. This favourable geological background results in an intense magnetic signal that permits the preparation and measurement of thin, around 3 mm-thick slice samples, each representing around 45 yr. The Characteristic Remanent Magnetization (ChRM), isolated after systematic stepwise Alternating Field demagnetization, is well defined, with Maximum Angular Deviation (MAD) generally lower than 10°. Paleomagnetic directional data allow the reconstruction of the PSV path during the Holocene for the area. Comparison of the new data with archeomagnetic data from Italian archeological artefacts and with the predictions of the SHA.DIF.14k and pfm9k.1a global geomagnetic field models shows that the Rio Martino flowstone represents an excellent recorder of the Earth's magnetic field during the last 10,000 years. The obtained high resolution paleomagnetic record, together with the high quality chronology, provide promising data both for the detection of short time geomagnetic field variations and for completing past regional PSV curves for the prehistoric period, for which well-dated data are still scarce.

Keywords: Paleosecular variation, Rock magnetism, Speleothem, Italy

1. Introduction

To investigate geomagnetic field behavior in the past and to explore its short-term features, high-resolution records from globally distributed archives of different origin are necessary (Mandea and

Olson, 2009). For Paleosecular Variation (PSV) reconstructions, an ideal paleomagnetic record should satisfy several requirements, such as having a stable remanent magnetization, being well dated, offering a continuous record and presenting high-time resolution. Even though several materials may satisfy some of these characteristics, the last two features of continuity and high-resolution are rarely coupled. Marine and lacustrine sediment sequences are archives most likely to ensure continuous records and have therefore been intensively studied to obtain geomagnetic data over long time scales (e.g. Turner and Thompson, 1981; Rolph et al., 2004; Vigliotti, 2006). However, sometimes data reliability may be questionable: the remanence acquisition mechanisms, the smoothing effects of bioturbation, the inclination error and the remanence acquisition delay are just some of the problems that may affect this kind of record. On the other hand, volcanic rocks and fired archeological artifacts may preserve very reliable paleomagnetic data but they are highly discontinuous in time. The age uncertainties of the volcanic products, as well as the lack of continuity and the limited time extension of available *in situ* archeological baked clay structures, restrict their use for high-resolution record studies.

Several research groups have studied speleothems for both PSV and paleoenvironmental reconstructions (e.g. Latham et al., 1989; Lean et al., 1995; Openshaw et al., 1997; Osete et al., 2012; Font et al., 2014), revealing their high potential for magnetic and secular variation reconstructions (Lascu and Feinberg, 2011). Paleomagnetic time series from speleothems, although still sparse, can provide excellent temporal resolution once the speleothem growth continuity and age range are recognized as, for example, in the case of the Mexican stalagmite studied in the pioneering work of Latham et al. (1986). The key feature of speleothems are that they can grow continuously for 10^3-10^5 yr and can be accurately dated by the uranium-series method (e.g. Richards and Dorale, 2003). They normally show little or no secondary alteration, and are generally easy to orient and sample (though with obvious consideration of natural heritage values).

Based on the magnetic properties, remanent magnetization of speleothems is mainly dominated by two mechanisms: it may be of detrital (DRM) and of chemical (CRM) origin (Lascu and Feinberg, 2011). Detrital input may be ascribed both to the flood and drip water percolations (Openshaw et al., 1997; Fairchild et al., 2006). No inclination error on the paleomagnetic record has been reported so far. Moreover, speleothems present the advantage to acquire their magnetization in a short time after their formation, entailing that the registered magnetic remanence variations reliably reflect the PSV path in the past. Nevertheless, all these promising features are contrasted by the speleothems' generally low concentration in magnetic minerals and thus their low magnetic signal that importantly limits their use in magnetic studies. To bypass this problem, large samples have been commonly used in paleomagnetic studies, reducing however the obtained time-resolution. Generally, a sample of around 2 cm may average ca 100-4000 yr (Strauss et al., 2013) and thus the obtained SV time-resolution is very low.

This paper reports the results of a paleomagnetic study performed on a flowstone sampled at Rio Martino Cave (North Western Alps, Italy). The favourable geologic context of the cave, which is mainly surrounded by meta-ophiolites, makes this flowstone very rich in detrital ferromagnetic components, and thus an ideal geomagnetic field recorder due to its high magnetic remanence properties. Although a high content of detrital material can compromise U/Th dating (Hellstrom, 2006), we have been able to produce a continuous, radiometrically-dated, directional SV record for the area during the last ~10 kyr, at a sampling resolution averaging 45 yr. Comparison of the new data with archeomagnetic data from Italian artifacts and with the predictions of regional and global geomagnetic field models, shows that the Rio Martino flowstone represents an excellent recorder of the Earth's magnetic field in the past and demonstrates the potential of speleothems for PSV studies and for the investigation of short-term variations of the geomagnetic field.

2. Geological setting and sampling

The Rio Martino Cave (44°42' N, 7°09' E) is located in the inner sector of the Western Alps (Northern Italy), which consists of a range of continental and oceanic tectono-metamorphic units bounded by major orogen-scale faulting (Balestro et al., 2014), and exhumed and stacked in the axial sector (Fig. 1).

The cave is developed within the Mesozoic carbonate cover of the Palaeozoic Dora Maira (Balestro et al., 2013). This unit is overlain by the Monviso meta-ophiolite complex, a major eclogized remnant of the Ligurian-Piedmont oceanic lithosphere, which in turn is tectonically overlain by the Queyras Schistes Lustrés, interpreted as a fossil accretionary wedge.

The surface above the cave is overlain mainly by glacial deposits. The cave is located at 1530 m a.s.l. on the right flank of the upper Po valley. It is a spring cave, ca. 3000 m long, with 200 m maximum elevation difference, and it is crossed by a small river with an average discharge of 50 l/s (maximum 200 l/s) (Badino and Chiri, 2005).

The presence of highly magnetized rocks in the cave's surroundings (Fig. 1) and the strong magnetic anomalies observed in the Monviso Massif area (Lanza and Meloni, 2006) could induce a magnetic deflection effect in the area. To evaluate the possible effect exerted by the meta-ophiolitic masses and to determine that it does not exert a significant influence on the paleomagnetic sampling, we used a triaxial fluxgate magnetometer to measure the geomagnetic field components outside, next to the entrance, and inside the cave. The computed magnetic inclination values of 60.7° (outside the cave) and 60.5° (on the flowstone surface) are fully comparable to the 2013 IGRF model of 60.6° (http://www.ngdc.noaa.gov/geomag-web). Besides, outside the cave we performed some orientation checks by using both the magnetic and the solar compass. The difference between the two declinations was small, ranging from -5° to +2°. Such differences are not significant and indicate that possible local magnetic effects on the paleomagnetic sampling can be considered negligible.

Two sampling campaigns were carried out to collect two cores from the same flowstone, which has accumulated on the side of a seasonally active stream with a high-detrital content. The cores were situated around 20-30 cm apart from one another and were cored using an adapted electric-powered drill. The first core (RMD1), sampled during the first campaign in 2010, was not azimuthally oriented. The second core (RMD8), sampled in 2013, was oriented *in situ* by magnetic compass and inclinometer. Each core was ca. 60 cm long and was drilled perpendicular to the flowstone growth axis.

A quarter of each core was dedicated to paleomagnetic analysis. The investigated sub-samples consisted of small slices, about 3 mm thick (varying from 2.5 to 4 mm), cut almost perpendicular to the speleothem's growth direction. Slicing was performed using a very thin amagnetic saw, which ensured that only 1 mm of material was consumed during the cut. Following this systematic sampling, we obtained 146 slices from RMD1 core and 143 from RMD8 core. Each slice was positioned in the centre of a non-magnetic plastic cylinder (2.5 cm diameter, 2.3 cm height) that allowed its handling as per standard paleomagnetic samples (Fig. 2).

3. Methods

3.1. U/Th dating and age modelling

Nineteen solid prisms of ~40 mg (~2 mm wide along the lamina and 1 mm thick on growth axis) from core RMD1 were used for age determination (Table S1 in Supplementary Material). The U/Th dating was performed at the University of Melbourne (Victoria, Australia) following the method of Hellstrom (2003). Briefly, samples were dissolved and a mixed ^{236}U-^{233}U-^{229}Th spike was added prior to removal of the carbonate matrix with ion-exchange resin. The purified U and Th fraction was introduced in a dilute nitric acid to a multi-collector inductively coupled plasma mass spectrometer (MC-ICPMS, Nu-Instruments Plasma). The $^{230}Th/^{238}U$ and $^{234}U/^{238}U$ activity ratios were calculated from the measured atomic ratios using an internally standardised parallel ion-counter procedure and calibrated against the HU-1 secular equilibrium standard. Correction for detrital Th content was applied using initial activity ratios of detrital thorium $(^{230}Th/^{232}Th)_i$ of 1.3 ± 0.45. This value, and its relative 2σ uncertainty, was calculated using a Monte Carlo 'stratigraphic constraint' procedure based on the series of U/Th ages (Hellstrom, 2006). A depth-age model was constructed using a Bayesian Monte Carlo approach following the method described by Drysdale et al. (2005) and Scholz et al. (2012).

3.2. SEM-EDS analysis

The mineralogy of the detrital inclusions in the studied flowstone was investigated by dissolving different portion of various thin slabs of the RMD1 core in diluted hydrochloric acid and passing the digests through 0.45 micrometre cellulose acetate filters. The residues, bearing almost all of the non-carbonate mineral inclusions contained in the speleothem, were observed and analysed with a Cambridge Stereoscan 360 Scanning Electron Microscope housed at the Earth Science Department of the University of Turin, Italy. Analyses were performed using an Oxford Inca X-Act 200 EDS microanalysis equipped with a Link Pentafet detector (thin window), allowing qualitative/quantitative determination of light elements (down to boron). All data were obtained at 15 kV HT, 25 mm WD, probe current range 800 pA – 1.2 nA and analysis time from 60 to 500 s. Primary standardization was performed on SPI Supplies and Polaron Equipment standards, and the system was regularly calibrated against a high-purity metallic Co standard before each experimental session. Data were processed with the Inca 200 Microanalysis Suite Software, version 4.08, and calibrated on natural mineral standards using the ZAF correction method. Analytical data are considered to be only semi quantitative due to the nature of the samples (rough surface of the particles, lack of horizontality, lack of surface polishing). A total of about 1500 analyses was performed on seven samples coming from different portions of the core, corresponding to about 200 measurements for each filter, randomly scattered on the filter surface for better representativeness.

Despite the results of magnetic analysis, very few magnetite particles were found in the filtered material, most likely because the single-domain magnetic particles (less than 200 nm diameter) were not retained by the 0.45 µm filter. Magnetite was indeed observed in sandy materials from Rio Martino, being found in the bed sediments of the relatively high-energy environment of the cave stream, rather than as detritus in carbonate flowstone speleothems.

3.3. Rock magnetic measurements

All magnetic measurements were performed at the ALP Paleomagnetic Laboratory (Peveragno, Italy). Rock magnetic experiments were performed on representative samples from both cores. Rock magnetism was investigated by low-field susceptibility (k_m) and natural remanent magnetization (J_r) measurements using a KLY3 kappabridge and a JR6 spinner magnetometer with a sensitivity of the order of 10^{-8} SI and 10^{-6} A/m, respectively. Susceptibility was measured at least five times per sample in order to calculate a mean value. Standard deviation is low and normally less than 5% of each mean susceptibility value for specimens associated with a susceptibility spike; uncertainty grows to 20-35% for the remaining specimens, with negative (diamagnetic) susceptibility values. All samples were weighed to get the mass-normalized susceptibility (χ, m^3kg^{-1}) and intensity (*J,* Am^2/Kg).

Isothermal Remanent Magnetization (IRM) curves were obtained with an ASC pulse magnetizer, applying stepwise increasing fields up to 1 T. Thermal demagnetization of a three-axis composite IRM was also performed on representative samples (Lowrie, 1990). An IRM was imparted with an ASC pulse magnetizer along the sample's three orthogonal axes, applying first a maximum 1.5 T, then a medium 0.3 T and finally a minimum 0.1 T magnetic field. Crossover plots of IRM curves and alternating field (AF) demagnetization of the saturation IRM (SIRM) were carried out to investigate the magnetic grain size (Symons and Cioppa, 2000).

All specimens were AF demagnetized stepwise up to 100 mT with a ASC-D 2000 equipment. Representative twin specimens were also thermally demagnetized stepwise with a Schonstedt TSD-1 furnace.

4. Results

4.1. Chronology

All the U/Th ages obtained from RMD1 were in stratigraphic order within the associated uncertainties, except for two samples which were rejected as outliers (Table S1 in Supplementary Material). Macroscopic and thin-section analyses of core RMD1 shows no growth interruption along its length. Age modelling performed on RMD1 core indicates that the flowstone grew continuously between 0.56 ± 0.06 ka and 9.7 ± 1.6 ka b2k (Fig. 3). The mean growth rate is 0.05830 mm/yr, which implies a mean time-resolution of ca. 60 yr (3 mm specimen + 1 mm cut) for the PSV record. The time averaged in each 3 mm slice sample is ca. 45 yr. The age of RMD8 was inferred by comparing clearly visible growth layers (Fig. 2a) between the two cores, associated with spikes in both the magnetic susceptibility and magnetization.

4.2. EDS

The mineralogy of the detrital portion in the RMD1 core is in strong accord with the composition of the surrounding lithology. Apart of the calcareous formation in which the cave is developed, the main rocks in the area are prasinites, amphibolites and serpentines. Minerals were grouped by similar chemistry, with some simplifications: as stated above, analyses were not fully quantitative, only semi-quantitative. The main identified groups are: iron oxides (without magnetite, identified apart by morphological features), magnesium silicates (other than serpentine), serpentine group, white mica group, feldspar, tremolite-actinolite amphiboles, other amphiboles (mainly hornblende), epidote group, chlorite group, quartz and accessories. The main minerals (Fig. 4) are represented by iron oxides (not distinguishable by chemistry for the reason explained above), magnesium silicates and serpentine group minerals. Iron oxides are mostly irregular in shape as if they had undergone reworking from the stream or by feedwater (Perkins, 1996). In few cases, a framboidal shape suggests *in situ* growth.

4.3. Magnetic mineralogy

The mass magnetic susceptibility of the specimens strongly varies. It mostly shows a prevailing diamagnetic phase with small negative values (from -7 to 0 x 10^{-9} m^3 kg^{-1} with a mean value of -4 x 10^{-9} m^3 kg^{-1}), alternating with high positive spikes, up to 970 x 10^{-9} m^3 kg^{-1}, suggesting a very low concentration of magnetic minerals in these specimens. Calcite bulk susceptibility is -12.09 μSI; its mass susceptibility is about -4.46 x 10^{-9} m^3 kg^{-1} (Almqvist et al., 2010). Since the literature value for the susceptibility of calcite refers to single crystal, we can assume that the mass susceptibility for calcite in the speleothem is slightly higher, because of mineral porosity. Assuming a constant diamagnetic contribution mostly due to calcite, the relative variability of magnetic susceptibility is indicative of variations of the concentration of magnetic minerals: a mean χ value of -4 x 10^{-9} m^3 kg^{-1} can be assumed to be representative of the "standard" content in magnetite, while high values represent for pulses of higher detrital input.

The natural magnetization intensity (J_r) strongly varies from specimen to specimen, being on average around 1-10 x 10^{-6} Am^2 kg^{-1} with spikes up to 80 x 10^{-6} Am^2kg^{-1}. The variations of these two bulk parameters are correlated; the computed correlation coefficients are r = 0.87 and r = 0.76 for RMD1 and RMD8, respectively. This corroborates the hypothesis that their values are essentially controlled by changes in concentration of the magnetic oxide.

IRM acquisition curves from representative samples saturate at relatively low field (around 0.3 T), indicating the presence of a low coercivity mineral (Fig. 5a). During the thermal demagnetization of the orthogonal IRM components (Lowrie, 1990), two typical behaviors were observed, which are independent of the magnetization intensity of the specimens. The first (e.g. sample RM68a), representing about the 80% of the measured specimens, suggests that the primary remanence is dominated by a soft magnetic carrier, demagnetized at ca 350-450 °C, which is interpreted as a titanomagnetite (Fig. 5b). The second (e.g. sample RM44a), in the remaining 20%, is characterized by a first drop in the magnetization intensity between 200 and 300 °C, which may be related to the existence of maghemite (Pan et al., 2000), even though this evidence is not sufficient to unambiguously identify this magnetic phase (Zhu et al., 2012).

The presence of (titano)magnetite of detrital origin is easily justified considering the geologic context of the cave and it is probably originated from the highly magnetic rocks of the surrounding area, mostly meta-ophiolites (Balestro et al., 2013). The occurrence of small serpentinite lithics was also detected. In those cases, the Median Destructive Field (MDF), which is normally stable and around 50-60 mT, drops to 5-25 mT. Deflections from MDF = 50 mT occur only where both the magnetic susceptibility and the magnetization intensity values are high. To check for these variations, we performed the experiment of Symons and Cioppa (2000) on some selected specimens, which were characterized by MDF ranging from 15 to 60 mT. It consists of a crossover plot, where the %SIRM is plotted as a function of the applied field, using a logarithmic scale (Fig. 5c). Results suggest that, except specimen SP212, which is characterized by MD (titano)magnetite, samples mainly contain SD to PSD (titano)magnetite grains.

The modified Lowrie-Fuller method (Johnson et al., 1975), which represents a valid first-order indicator of grain-size composition (Font et al., 2014), was applied on some specimens with MDF in the range 45-50 mT. Results always show L-type behaviors with the Anhysteretic Remanent Magnetization (ARM) dominating the Isothermal Remanent Magnetization (IRM) during AF demagnetization treatment, corroborating the occurrence of SD grains.

5. Paleomagnetic directions

5.1. Natural Remanent Magnetization and the Anisotropy of Remanent Magnetization

Speleothems can potentially offer very useful records of PSV and the remanence acquisition mechanisms in speleothems were studied in detail (e.g., Lascu and Feinberg, 2011; Strauss et al., 2013, and reference therein). In order to provide a reliable PSV record, the magnetization should be acquired and locked soon after the calcium carbonate film deposition on the drip surface of a speleothem (almost instantaneously). Following Strauss et al. (2013), lock-time for a speleothem is sub-annual and the magnetization is a DRM. Synchronicity between crystallization and magnetization has been tested experimentally by synthetic stalagmite growth (Morinaga et al., 1989), confirming the short time-lapse in acquiring magnetization parallel to the ambient field direction.

To test if this requirement is encountered in Rio Martino flowstone and thus to check for its reliability as a PSV recorder, we measured the Anisotropy of Isothermal Remanent Magnetization (AIRM) on two selected sets of samples from RMD1 (azimuthally non-oriented), each comprising a time interval of ca 1000 yrs. The first set comprised 16 samples (SP200 to SP260) from 4.26 ± 0.23 to 3.30 ± 0.03 ka, and the second set 14 samples (SP346 to SP397) from 7.76 ± 0.12 to 6.91 ± 0.11 ka). A difference of 20° in the mean magnetic ChRM inclination distinguished these two sets of specimens. Each specimen was first AF demagnetized using a tumbling 2G demagnetizer at 60 mT peak field and then given an isothermal remanent magnetization (IRM) with a steady field of 20 mT using an AGICO PUM-1 pulse magnet. After measurement with the spinner magnetometer, the sequence was repeated for a total of 12 different orientations of the IRM in order to calculate the anisotropy tensor. The experiment (Fig. 6) shows that for both sets, the maximum IRM anisotropy axis I_1 is concordant or statistically indistinguishable from the mean ChRM direction, showing no relation with the speleothem growth laminae. This shows that ChRM direction is due to the statistical alignment of the magnetic particle and fully agrees with the conclusions of Zhu et al. (2012), who performed both anisotropy of magnetic susceptibility (AMS) and AIRM on stalagmites. They found that the AMS was dominated by the calcite fabric, being the minimum susceptibility axis k_3 aligned perpendicular to the stalagmite growth laminae, while the AIRM fabric showed the maximum remanence axis I_1 almost parallel to the NRM direction. All these data point to a detrital origin of the magnetization, with the geomagnetic field control in the orientation of the ferromagnetic minerals.

5.2. Characteristic Remanent Magnetization determination

Demagnetization results are represented by intensity-decay curves and plotted in Zijderveld diagrams (Fig. 7). Most of the specimens are characterized by a small viscous remanent magnetization (VRM), which is easily removed at AF field of 15-20 mT. The remaining demagnetization path is linear and points to the origin, indicating a stable remanent magnetization; this component has been interpreted as the Characteristic Remanent Magnetization (ChRM). The ChRM direction is mostly well defined and characterized by low MAD values (lower than 8^{o} for the 91% of the studied samples). AF and thermal demagnetization results obtained from twin specimens are very similar (Fig. 7), confirming the reliability of the ChRM direction (Fig. 8; Table S2 in Supplementary Material). The AF demagnetization treatment has been preferred rather than the thermal demagnetization, as it permits the further use of the same samples for paleoenvironmental and relative paleointensity investigations through Anhysteretic Remanent Magnetization (ARM) measurements. Therefore, all samples were systematically AF demagnetized and ChRM directions were obtained from the AF demagnetization results. Demagnetization behavior in samples with low- and high-remanence (spike) does not change significantly except for specimens where serpentinite clasts were recognized.

6. Directional Paleosecular Variation during Holocene

Paleomagnetic directions obtained from the two cores (reported in Table S2 of Supplementary material) are plotted versus depth from the top of the core in Figure 9. Some spikes in declination show a strong correspondence with atypical MDF values, lower/higher than 20/60 mT. These deflected directions have been ascribed to the presence of small serpentinite lithic fragments and thus rejected. The declination of core RMD1, which is not azimuthally oriented, has been recovered after adjustment of its mean value to the Geocentrical Axial Dipole (GAD) calculated at Rio Martino according to the following procedure: first the RMD1 core's mean direction has been calculated for the last 10 kyr and then its deviation from the GAD value has been computed. The difference in declination between the core and the GAD has been extracted from each declination value of the RMD1 core.

Generally, directions obtained from both RMD1 and RMD8 cores are in good agreement with each other and data reproducibility is high (fig. 9). This is particularly evident for the inclination data at depths between 200.0 and 600.0 mm, where the two records match each other. Instead, in some cases, mostly at depths from 150.0 to 200.0 mm, differences in inclination of around 20°-25° are observed. The cause of such differences is not clear, even though uncertainties during sampling (slices not perfectly perpendicular to the flowstone growth) and deflections related to a possible anisotropy effect connected to the calcite crystals growth cannot be completely excluded. To guarantee the high quality of the new data, only ChRM directions characterized by MAD values lower than 6^{o} have been used in the plots.

The paleosecular variations registered by the Rio Martino speleothem are compared with spot archeomagnetic directions obtained from dated archeological structures from Italy. The Italian archeomagnetic dataset (Tema et al., 2006; Tema, 2011) has been updated by some recently published results (Malfatti et al., 2011; Kapper et al., 2014; Tema et al., 2013; 2014; 2015; 2016) and all data have been relocated at the geographic coordinates of Rio Martino via the virtual geomagnetic pole method (Noel and Batt, 1990). The comparison shows that the archeomagnetic data generally fit very well to the speleothem directions (Fig. 10). Some discrepancies can be observed around 1000 AD, mainly regarding the speleothem's declination values that are lower compared to those obtained from archeological materials. Nevertheless, it is particularly interesting to note that for the BC period, the available archeomagnetic data, even if very limited and often accompanied by large error bars, are in excellent agreement with the new data. This confirms the high potential of Rio Martino speleothems to continuously and reliably register the

Earth's magnetic field, offering a unique source of high quality data for the BC period where *in situ* archeological artifacts are very scarce.

The new data are also compared with the predictions of global geomagnetic field models. Here, we have used for comparison the pfm9k.1a (Nilsson et al., 2014) and the SHA.DIF.14k (Pavón-Carrasco et al., 2014) models that are the most recently published global geomagnetic models that cover the Holocene period. Comparison shows good agreement between the speleothem records and the global models predictions, confirming some interesting features of the Earth's magnetic field in the past. The eastward declinations around 1000 BC mainly observed in the SHA.DIF.14k model are well sustained by the speleothem data for the same time period, that show high declination values too. For the 4000-2000 BC period only small declination variations are shown by the speleothem data, in agreement with the pfm9k model's predictions, while the declination peaks seen in the SHA.DIF.14k model (e.g. around 3600 BC) are not confirmed by the speleothem data. For periods older than 5000 BC, speleothem records show generally higher declination values compared to the models predictions and other archeomagnetic data. Regarding the inclination data, excellent agreement can be observed for the periods 6000-3500 BC and 500 BC-500 AD. However, around 1000 BC, speleothems show an interesting high inclination peak that is not observed in the models or sustained by the available archeomagnetic data. This peak is actually only observed on the data from the RMD8 core and definitely more independent records are necessary to investigate if it corresponds to a real abrupt directional change (as it corresponds also to high declination values) of the geomagnetic field at this time period. For the 7500 BC to 6500 BC period, the speleothem records show continuously increasing inclination with a peak around 6500 BC that seems to be in agreement with the pfm9k model.

7. Conclusions

Some outstanding characteristics of the Rio Martino flowstone, such as its continuous growth, the well-constrained chronology and the intense magnetic signal, make its paleomagnetic directional record for the Holocene in the northwestern Italy particularly appropriate for PSV investigation. The high magnetic signal permits a high-resolution record of around 60 yr per data point; the regular scatter of paleomagnetic data through time shows an almost constant distribution of directional data though the Holocene.

The obtained directional results are well defined and offer a unique, almost continuous, secular variation record for the last 10000 years. Although some discrepancies can be observed, comparison with archeomagnetic data and global geomagnetic field models confirms the high potential of these speleothems to the reconstruction of the Earth's magnetic field variations in the past.

Our results show that the Rio Martino flowstones are not affected by recrystallization effects or secondary alterations. The speleothems do not show any inclination shallowing when compared with model predictions, and in some cases show high inclination peaks that are not observed by the models (e.g. around 3800 BC, 1000 BC, 800 AD).

The record characteristics overcome some typical features affecting both clastic sedimentary and the archeomagnetic PSV records, including the smoothness of the magnetic data in the case of the former and the presence of temporal gaps and uneven data distribution in the case of the latter.

The high resolution obtained points to the possibility of detecting short and abrupt geomagnetic field changes by studying a wide variety of Earth Magnetic Field variations at a timescale from tens of years to the tens of centuries. The use of speleothem records for PSV reconstructions can be particularly important for the prehistoric period where other sources if data coming from archeological artifacts or well dated volcanic eruptions are scarce.

Acknowledgments

We thank the Associazione Gruppi Speleologici Piemontesi (AGSP) for the logistical support during field campaign and in particular Raffaella Zerbetto for her kindness and competence. This paper is dedicated to the memory of Prof. Roberto Lanza who enthusiastically supported this study during the last months of his life giving fundamental advices and suggestions.

References

Almqvist, B.S.G., Herwegh, M., Schmidt, V., Pettke, T., Hirt, A.M., 2010. Magnetic susceptibility as a tool to study deformed calcite with variable impurity content. Geochemistry Geophysics Geosystems, 11, Q01Z09, doi:10.1029/2009GC002900

Badino, G., Chiri, M., 2005. First data from the underground metereological station of Rio Martino, Italy. Hellenic Speleological Society. 21-28 August 2005, Kalamos, Greece.

Balestro, G., Fioraso, G., Lombardo, B., 2013. Geological map of the Monviso massif (Western Alps). Journal of Maps, 9, 4, 623-634, doi: 10.1080/17445647.2013.842507

Balestro, G., Festa, A., Tartarotti, P., 2014. Tectonic significance of different block-in-matrix structures in exhumed convergent plate margins: examples from oceanic and continental HP rocks in Inner Western Alps (northwest Italy). International Geology Review. DOI: 10.1080/00206814.2014.943307.

Drysdale, R.N., Zanchetta, G., Hellstrom, J.C., Fallick, A.E., Zhao, J.X., 2005. Stalagmite evidence for the onset of the Last Interglacial in southern Europe at 129+/−1 ka. Geophysical Research Letters 32, 1–4.

Fairchild, I.J., Smith, C.L., Baker, A., Fuller, L., Spötl, C., Mattey, D., McDermott, F., 2006. Modification and preservation of environmental signals in speleothems. Earth Science Reviews, 75, 105-153, doi:10.1016/j.earscirev.2005.08.003

Font, E., Veiga-Pires, C., Pozo, M., Carvallo, C., de Siqueira Neto, A.C., Camps, P., Fabre, S., Mirão, J., 2014. Magnetic fingerprint of southern Portuguese speleothems and implications for paleomagnetism and environmental magnetism. Journal of Geophysical Research, 119, 7993-8020, doi:10.1002/2014JB011381.

Hellstrom, J.C., 2003. Rapid and accurate U/Th dating using parallel ion-counting multicollector ICP-MS. Journal of Analytical Atomic Spectrometry 18, 1346–1351

Hellstrom, J.C., 2006. U-Th dating of speleothems with high initial 230Th using stratigraphical constraint. Quaternary Geochronology, 1, 289-295.

Johnson, H.P., Lowrie, W., Kent, D.V., 1975. Stability of Anhysteretic Remanent Magnetization in fine and coarse magnetite and maghemite particles. Geophysical Journal of the Royal astronomical Society, 41, 1-10.

Kapper, L., Anesin, D., Donadini, F., Angelucci, D., Cavulli, F., Pedrotti, A., Hirt, A., 2014. Linking site formation processes to magnetic properties. Rock and archaeomagnetic analysis of the combustion levels at Riparo Gaban (Italy). Journal of Archaeological Science, 41, 836-855.

Lanza, R., Meloni, A., 2006. The Earth's Magnetism. An Introduction for Geologists. Springer,278 pp.

Lascu, I., Feinberg, J.M., 2011. Speleothem magnetism. Quaternary Science Reviews, 30, 3306-3320.

Latham, A.G., Schwarcz, H.P, Ford, D.C., 1986. The paleomagnetism and U-Th dating of Mexican Stalagmite, Das2. Earth Planetary Science Letters, 79, 195-207.

Latham, A. G., Ford, D.C., Schwarcz, H.P., Birchall, T., 1989. Secular variation from Mexican stalagmites: Their potential and problems. Physics of the Earth and Planetary Interiors, 56, 34–48.

Lean, C.B., Latham, A.C., Shaw, J., 1995. Palaeosecular variation from a Vancouver Island Stalagmite and comparison with Contemporary North American records. J. Geomag. Geoelectr., 47, 71-87.

Lowrie, W., 1990. Identification of ferromagnetic minerals in a rock by coercivity and unblocking temperature properties. Geophysical Research Letters, 17, 159-162.

Malfatti, J., Principe, C., Gattiglia, G., 2011. Archeaomagnetic investigation of a metallurgical furnace in Pisa (Italy). Journal of Cultural Heritage, 12, 1-10.

Mandea, M., Olsen, N., 2009. Geomagnetic and Archeomagnetic Jerks: Where Do We Stand? Eos, Transactions, American Geophysical Union, 90, 24, 208-208.

Morinaga, H., Inokuchi, H., Yaskawa, K., 1989. Palaeomagnetism of stalagmites (speleothems) in SW Japan. Geophys. J., 96, 519-528.

Nilsson, A., Holme, R., Korte, M., Suttie, N., Hill, M., 2014. Reconstructing Holocene geomagnetic field variation: new methods, models and implications. Geophysical Journal International, 198, 1, 229-248.

Noel, M., Batt, C.M., 1990. A method for correcting geographically separated remanence directions for the purpose of archaeomagnetic dating. Geophysical Journal International, 102, 753-756.

Openshaw, S., Latham, A., Shaw, J., 1997. Speleothem Palaeosecular Variation Records from China: Their contribution to the coverage of Holocene Palaeosecular Variation Data in East Asia. J. Geomag. Geoelectr., 49,485-505.

Osete, M. L., Martin-Chivelet, J., Rossi, C., Edwards, R.L., Egli, R., Munoz-Garcia, M.B., Wang, X.F., Pavon-Carrasco, F.J., Heller, F., 2012. The Blake geomagnetic excursion recorded in a radiometrically dated speleothem. Earth Planetary Science Letters, 353, 173–181.

Pan, Y., Zhu, R., Banerjee, S.K., Gill, J., Williams, Q., 2000. Rock magnetic properties related to thermal treatment of siderite: behaviour and interpretation. Journal of Geophysical Research, 105, 783-794.

Pavón-Carrasco, F.J., Osete, M.L., Torta, J.M., De Santis, A., 2014. A geomagnetic field model for the Holocene based on archaeomagnetic and lava flow data. Earth Planetary Science Letters, 388, 98 - 109.

Perkins, A.M., 1996. Observations under microscopy of magnetic minerals extracted from speleothems. Earth and Planetary Science Letters, 139, 281-289.

Richards, D.A., Dorale, J.A., 2003. Uranium-series chronology and environmental applications of speleothems. Review in Mineralogy and Geochemistry, 52, 407-460.

Rolph, T.C., Vigliotti, L., Oldfield, F. 2004. Mineral magnetism and geomagnetic secular variation of marine and lacustrine sediments from central Italy: timing and nature of local and regional Holocene environmental change. Quaternary Science Review, 23, 1699–1722.

Scholz, D., Hoffmann, D.L., Hellstrom, J., Bronk Ramsey, C., 2012. A comparison of different methods for speleothem age modelling. Quaternary Geochronology. 14, 94–104.

Strauss, B.E., Strehlau, J.H., Lascu, I., Dorale, J.A., Penn, R.L., Feinberg, J.M., 2013. The origin of magnetic remanence in stalagmites: observations from electron microscopy and rock magnetism. Geochemistry Geophysics Geosystems, 14, doi: 10.1002/2013GC004950

Symons, D.T.A., Cioppa, M.T., 2000. Crossover Plots: a useful method for plotting SIRM data in paleomagnetism. Geophysical Research Letters, 27 (12), 1779-1782.

Tema, E., 2011. Archaeomagnetic Research in Italy: Recent achievements and future perspectives. In: The Earth's Magnetic Interior, IAGA Special Sopron Book Series, Volume 1, Chapter 15, pp. 213-233. Eds: Petrovsky, E., Herrero-Bervera, E., Harinarayana, T., Ivers, D., Springer, doi: 10.1007/978-94-007-0323-0_15.

Tema, E., Hedley, I., Lanos, Ph., 2006. Archaeomagnetism in Italy: A compilation of data including new results and a preliminary Italian Secular Variation curve. Geophysical Journal International, 167, 1160-1171.

Tema, E., Fantino, F., Ferrara, E., Lo Giudice, A., Morales, J., Goguitchaichvili, A., Camps, P., Barello, F., Gulmini, M., 2013. Combined archaeomagnetic and thermoluminescence study of a brick kiln excavated at Fontanetto Po (Vercelli, Northern Italy). J. Arch. Science, 40 (4), 2025-2035.

Tema, E., Fantino, F., Ferrara, E., Allegretti, S., Lo Giudice, A., Re, A., Barello, F., Vella, S., Cirillo, L., Gulmini, M., 2014. Archaeological, archaeomagnetic and thermoluminescence investigation of a baked clay kiln excavated at Chieri, northern Italy: contribution to the rescue of our cultural heritage. Annals of Geophysics, 57, 5, G0548.

Tema, E., Camps, P., Ferrara, E., Poidras, T., 2015. Directional results and absolute archaeointensity determination by the classical Thellier and the multi-specimen DSC protocols for two kilns excavated at Osterietta, Italy. Studia Geophysica Geodaetica, 59, 554-577.

Tema, E., Ferrara, E., Camps, P., Conati Barbaro, C., Spatafora, S., Carvallo, C., Poidras, Th., 2016. The Earth's magnetic field in Italy during the Neolithic period: New data from the Early Neolithic site of Portonovo (Marche, Italy). Earth and Planetary Science Letters, 448, 49-61.

Turner, G.M., Thompson, E., 1981. Lake sediment record of the geomagnetic secular variation in Britain during Holocene times. Geophysical Journal of the Royal Astronomical Society, 65 (3), 703-725.

Vigliotti, L., 2006. Secular variation record of the Earth's magnetic field in Italy during the Holocene: constraints for the construction of a master curve. Geophys. J. Int., 165, 414–429.

Zhu, Z., Zhang, S., Tang, C., Li, H., Xie, S., Ji, J., Xiao, G., 2012. Magnetic fabric of stalagmites and its formation mechanism. Geochemistry Geophysics Geosystems, 13, doi: 10.1029/2011GC003869.

Figure Caption

Figure 1. a) Structural sketch map of the Western Alps; b) 3D reconstruction of the Inner Western Alps in the Rio Martino zone (modified after Balestro et al., 2014). The square indicates the location of the Rio Martino Cave.

Figure 2. a) The RMD8 core; b) a part of the flowstone systematically cut and sampled in 3 mm-high slices; c) the amagnetic plastic cylindrical holder created in order to fix the small samples in the centre of the cylinder and treat them as standard palaeomagnetic samples.

Figure 3. Age-depth model for RMD1 core. The age is expressed in b2k (before 2 ka).

Figure 4. The distribution of the mineral species in the detrital part of Rio Martino speleothem. The picture is the sum of ca 1500 EDS determinations from seven different portions from the same core. The “accessory minerals” include all the species <2,5 % of the analyzed particles, for each sample. The group includes rutile, zircon, monazite, apatite (mainly apatite-F), sphene, xenotyme, galena, pirite, ilmenite, barite.

Figure 5. a) Isothermal remanent magnetization (IRM) acquisition curves; b) thermal demagnetization of a composite three-axes IRM (Lowrie, 1990); c) crossover plots (Symons and Cioppa, 2000).

Figure 6. Equal area stereographic projections of the principal isothermal remanent magnetization axes and ChRM directions for specimens from a) SP200 to SP260, and b) SP346 to SP397.

Figure 7. Thermal and AF demagnetization results from twin specimens from samples a-b) RM7 and c-d) RM20 plotted in intensity decay plots (left) and Zijderveld diagrams (right). Symbols: full dots = declination; open dots = apparent inclination.

Figure 8. Equal area projections of the ChRM directions for five samples obtained from a) AF and b) thermal demagnetization on twin specimens. The star represents the mean value calculated for each group of samples following a Fisherian distribution.

Figure 9. a) Declination and b) inclination data from cores RMD1 (red) and RMD8 (blue) plotted versus depth in mm from the top of the core.

Figure 10. a) Declination and b) inclination plots of the new speleothem data (grey dots) together with the Italian archaeomagnetic data (red diamonds) and the pfm9k (green line) and SHA.DIF.14k (blue line) global geomagnetic field models. All directions are calculated at the geographic coordinates of Rio Martino (44.7^{o} N, 7.15^{o} E). Age is given both as Calendar Age (year AD) and b2k (before 2 ka).

Table caption

Table S1. Corrected U/Th ages for RMD1 core. The activity ratios have been standardized to the HU-1 secular equilibrium standard, and ages calculated using decay constants of 9.195×10^{-6} (^{230}Th) and 2.835×10^{-6} (^{234}U). Depths are from top, whilst the numbers in brackets are the 95% uncertainties.

Table S2. Characteristic remanent magnetization directions (ChRMs) of the samples from the RMD1 (left) and RMD8 (right) cores. Legend: z = depth in mm from the core top; D, I = magnetic declination and inclination; MAD = Mean Angular Deviation; D_{corr} = declination corrected by subtracting the angular difference between the $D_{GAD} = 0°$ and the mean ChRM declination (D = 146.1°).

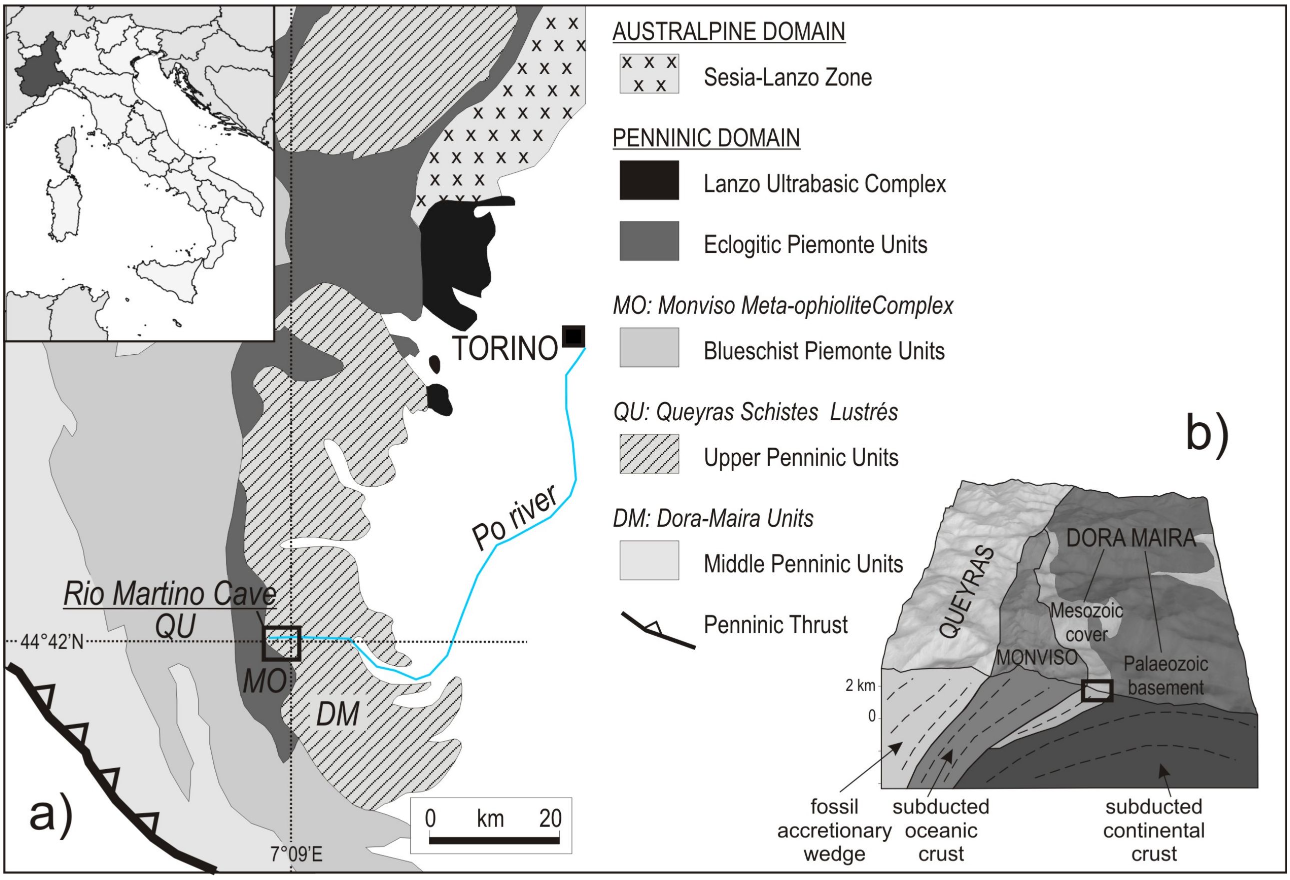
AUSTRALPINE DOMAIN
Sesia-Lanzo Zone
PENNINIC DOMAIN
Lanzo Ultrabasic Complex
Eclogitic Piemonte Units
MO: Monviso Meta-ophioliteComplex
Blueschist Piemonte Units
QU: Queyras Schistes Lustrés
Upper Penninic Units
DM: Dora-Maira Units
Middle Penninic Units
Penninic Thrust
TORINO
Po river
Rio Martino Cave
QU
MO
DM
44°42'N
7°09'E
0 km 20
a)
b)
QUEYRAS
DORA MAIRA
Mesozoic cover
MONVISO
Palaeozoic basement
2 km
0
fossil accretionary wedge
subducted oceanic crust
subducted continental crust

Fig. 1

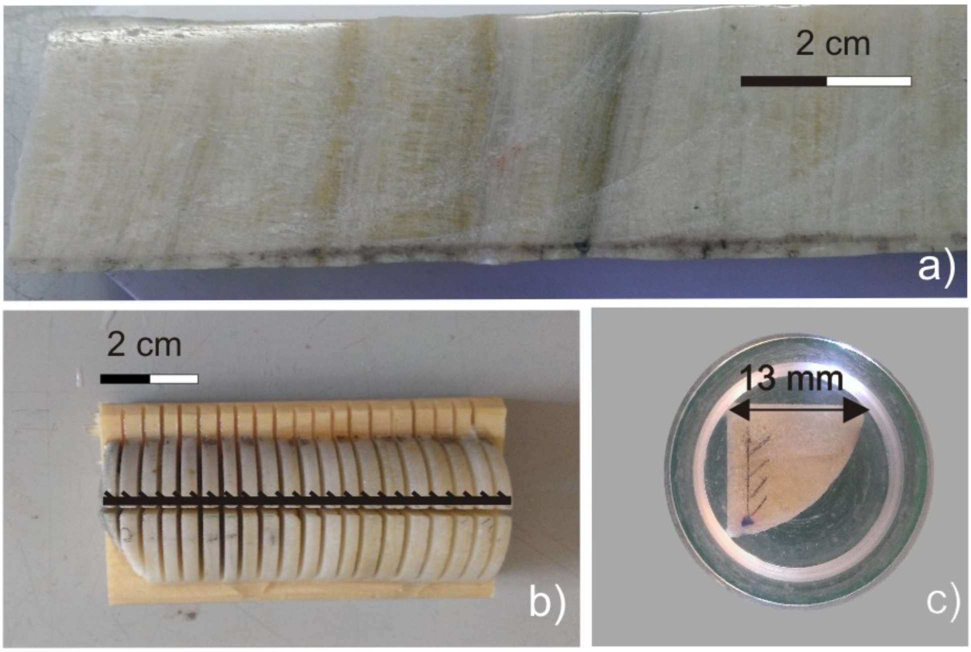

Fig. 2

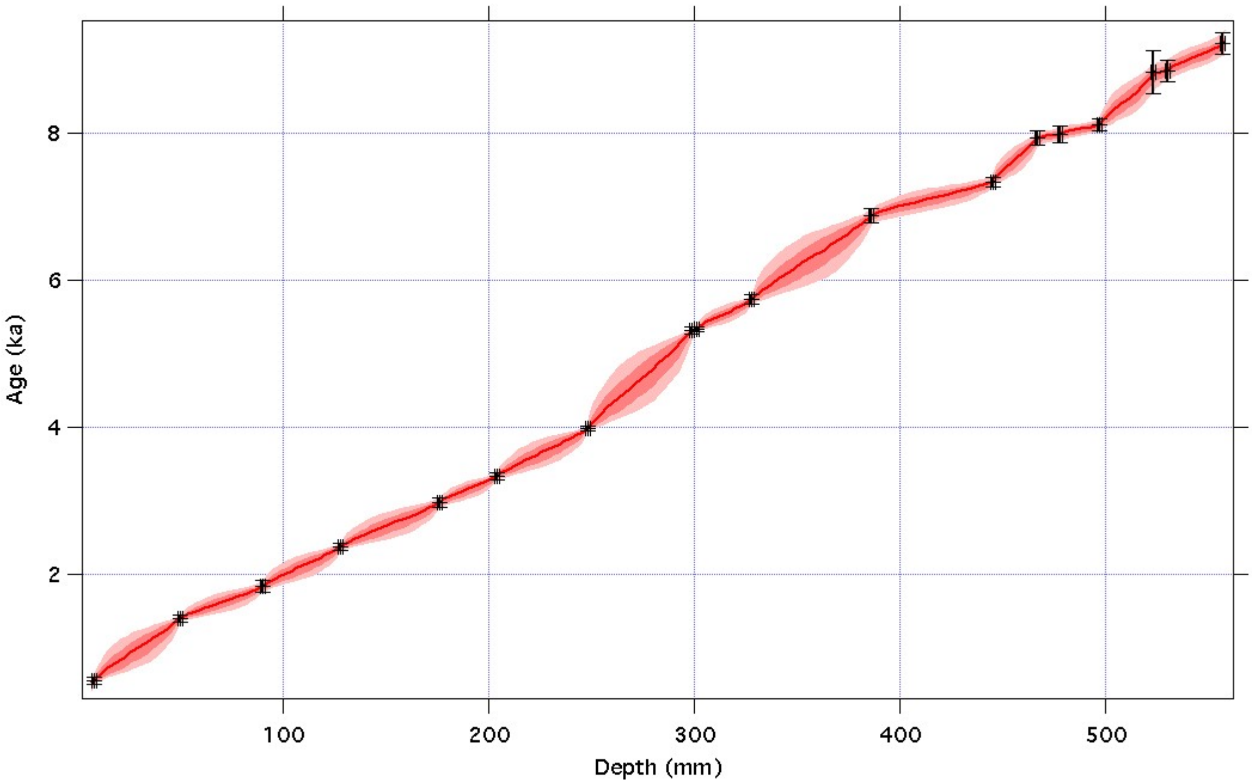

Fig. 3

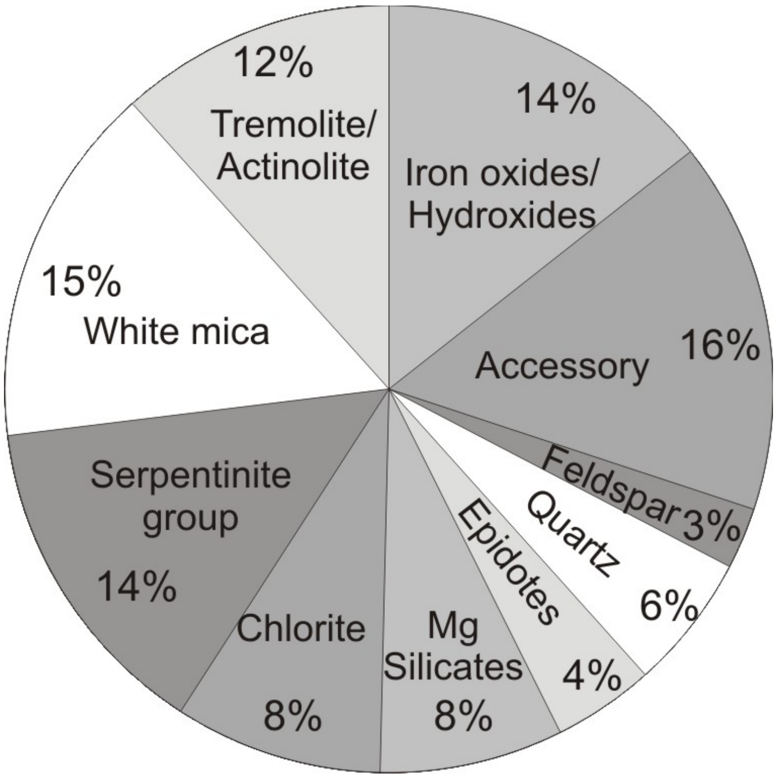
12%
Tremolite/
Actinolite
14%
Iron oxides/
Hydroxides
15%
White mica
Accessory
16%
Serpentinite
group
14%
Feldspar
3%
Quartz
6%
Epidotes
4%
Chlorite
8%
Mg
Silicates
8%

Fig.4

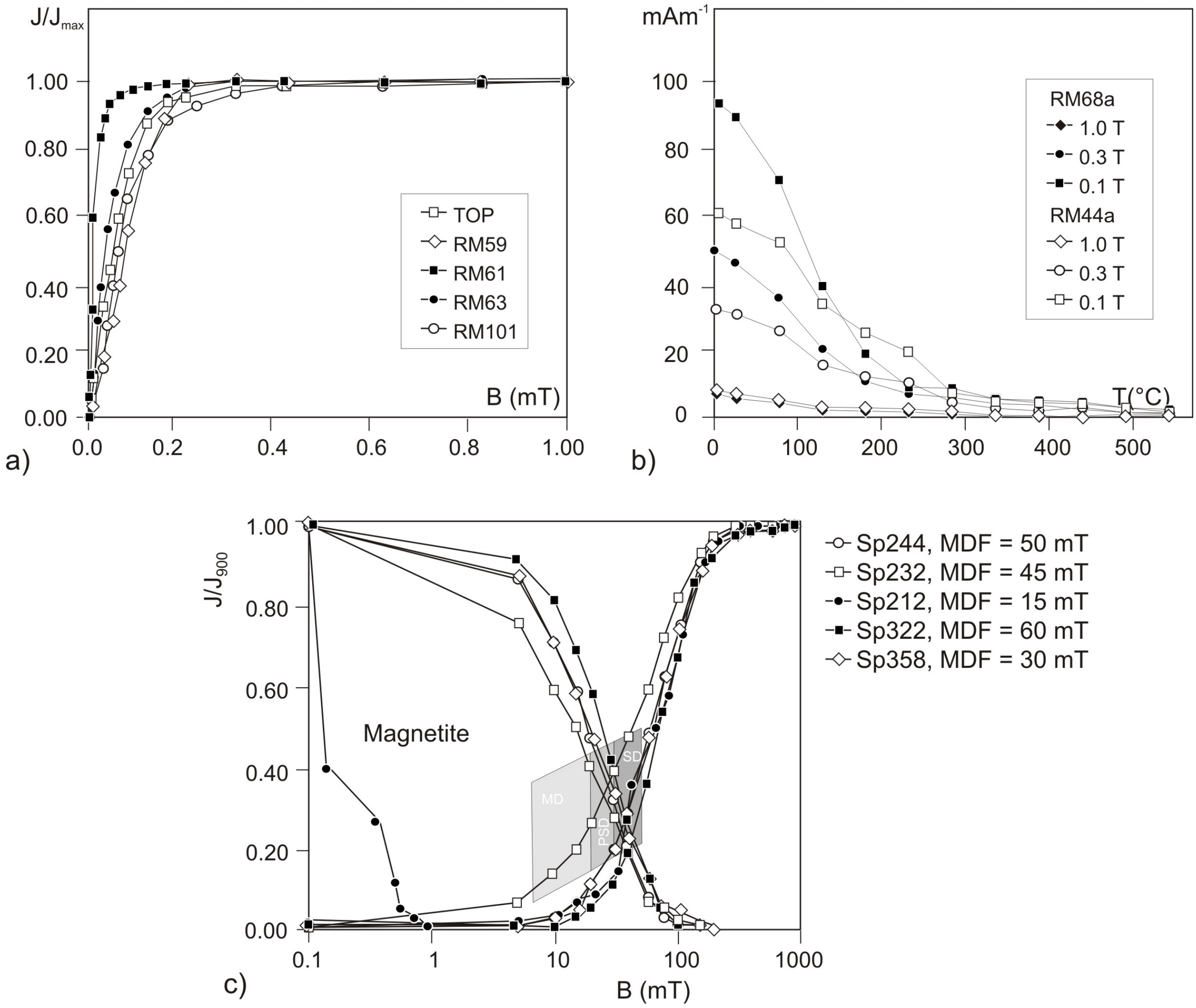

J/J$_{max}$
1.00
0.80
0.60
0.40
0.20
0.00
0.0
0.2
0.4
0.6
0.8
1.00
B (mT)
TOP
RM59
RM61
RM63
RM101
a)
mAm^{-1}
100
80
60
40
20
0
0
100
200
300
400
500
T(°C)
RM68a
1.0 T
0.3 T
0.1 T
RM44a
1.0 T
0.3 T
0.1 T
b)
J/J$_{900}$
1.00
0.80
0.60
0.40
0.20
0.00
0.1
1
10
100
1000
B (mT)
Magnetite
MD
PSD
SD
Sp244, MDF = 50 mT
Sp232, MDF = 45 mT
Sp212, MDF = 15 mT
Sp322, MDF = 60 mT
Sp358, MDF = 30 mT
c)

Fig. 5

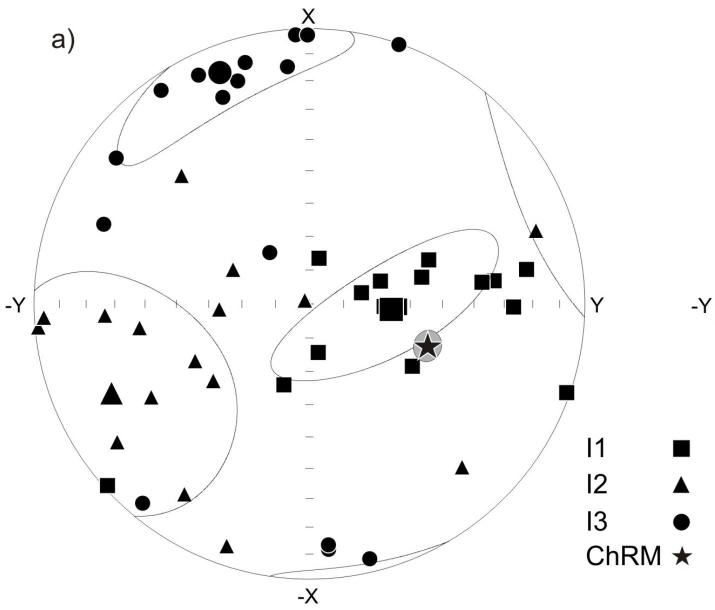

Fig. 6

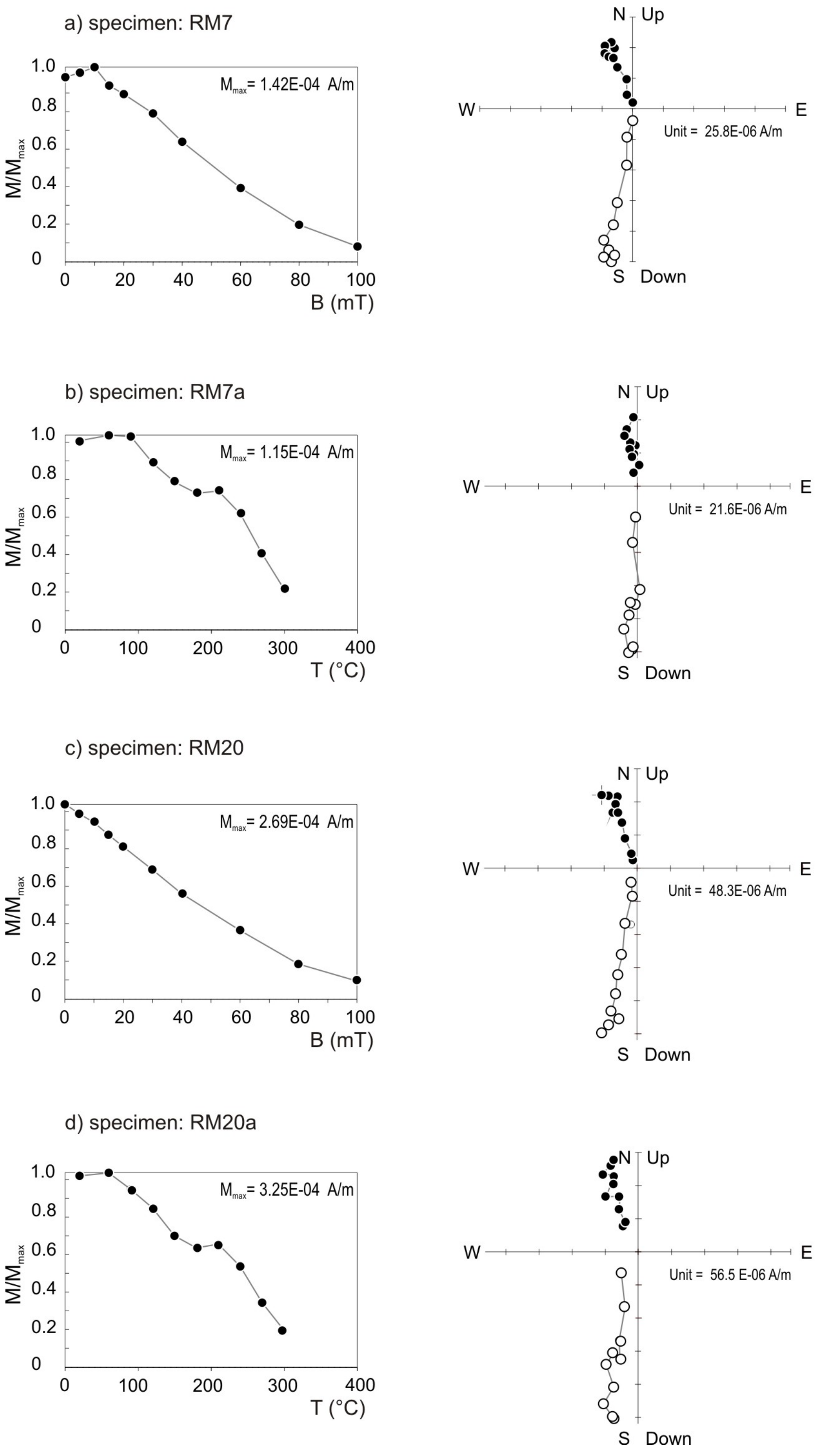
a) specimen: RM7
M_{max}= 1.42E-04 A/m
M/M_{max}
B (mT)
N Up
W
E
Unit = 25.8E-06 A/m
S Down
b) specimen: RM7a
M_{max}= 1.15E-04 A/m
M/M_{max}
T (°C)
N Up
W
E
Unit = 21.6E-06 A/m
S Down
c) specimen: RM20
M_{max}= 2.69E-04 A/m
M/M_{max}
B (mT)
N Up
W
E
Unit = 48.3E-06 A/m
S Down
d) specimen: RM20a
M_{max}= 3.25E-04 A/m
M/M_{max}
T (°C)
N Up
W
E
Unit = 56.5 E-06 A/m
S Down

Fig. 7

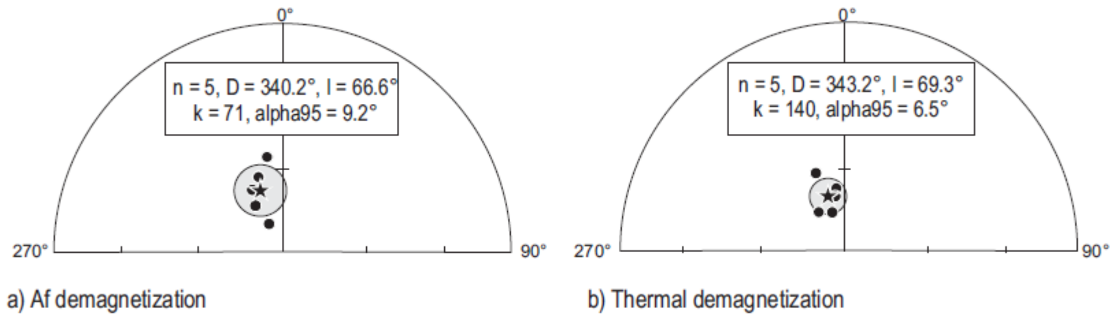
0°
n = 5, D = 340.2°, I = 66.6°
k = 71, alpha95 = 9.2°
270°
90°
a) Af demagnetization
0°
n = 5, D = 343.2°, I = 69.3°
k = 140, alpha95 = 6.5°
270°
90°
b) Thermal demagnetization

Fig. 8

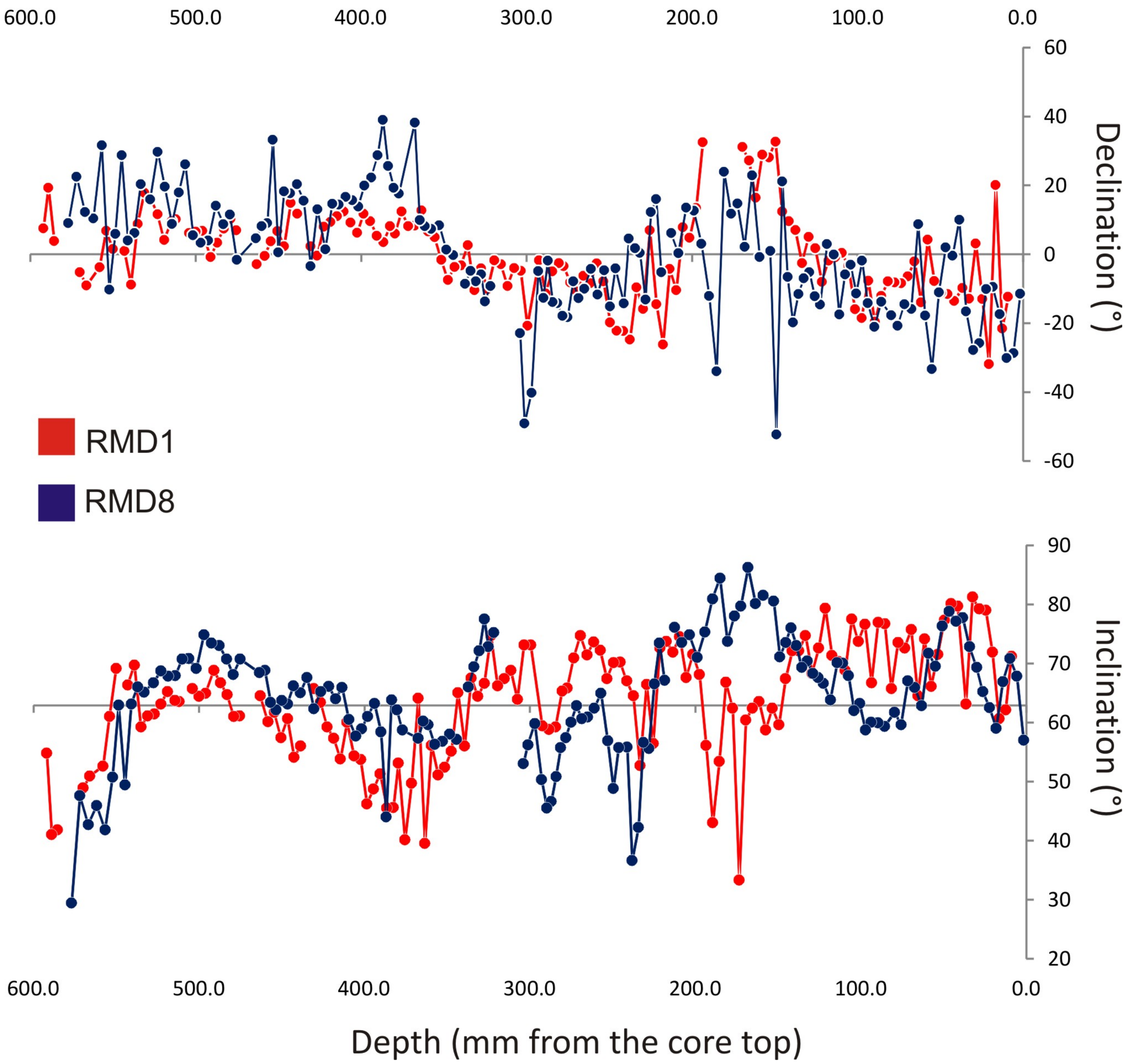

RMD1
RMD8
Declination (°)
Inclination (°)
Depth (mm from the core top)
600.0
500.0
400.0
300.0
200.0
100.0
0.0
60
40
20
0
-20
-40
-60
90
80
70
60
50
40
30
20

Fig. 9

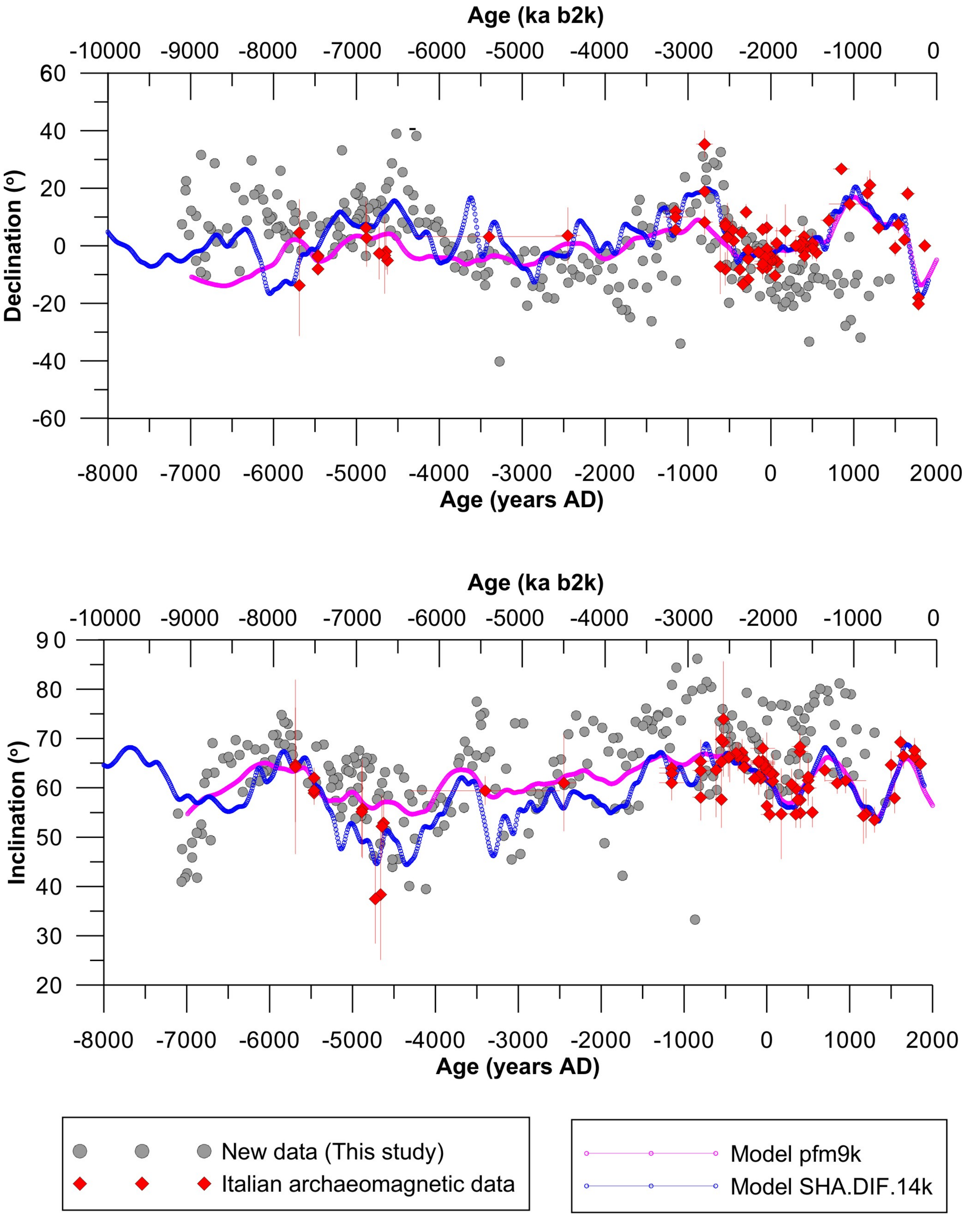
Age (ka b2k)
-10000
-9000
-8000
-7000
-6000
-5000
-4000
-3000
-2000
-1000
0
60
40
20
0
-20
-40
-60
Declination (°)
-8000
-7000
-6000
-5000
-4000
-3000
-2000
-1000
0
1000
2000
Age (years AD)
Age (ka b2k)
90
80
70
60
50
40
30
20
Inclination (°)
Age (years AD)
New data (This study)
Italian archaeomagnetic data
Model pfm9k
Model SHA.DIF.14k

Fig. 10

Sample ID	^{238}U (ng/g)	Depth (mm)	$^{230}Th/^{238}U$	$^{232}Th/^{238}U$	$^{230}Th/^{232}Th$	**Age cr Ka**	2se (ka)
RMD1-A	579	8.00	0.0082	0.001353	6.1	**0.553**	0.043
RMD1 137.5	885	50.00	0.0180	0.001229	14.7	**1.396**	0.046
RMD1 130.4	898	90.00	0.0252	0.002922	8.6	**1.825**	0.074
RMD1 126	773	128.00	0.0288	0.000870	33.1	**2.366**	0.048
RMD1 128.6	1124	176.00	0.0377	0.002149	17.5	**2.970**	0.068
RMD1 135.6	726	204.00	0.0394	0.000253	155.3	**3.328**	0.053
RMD1 133.5	1097	248.00	0.0478	0.000792	60.4	**3.969**	0.040
*RMD1 139.6**	*683*	*289.00*	*0.0815*	*0.026757*	*3.0*	***4.220***	*0.694*
RMD1-B	1135	299.00	0.0622	0.000642	96.9	**5.308**	0.058
RMD1-301	971	301.00	0.0613	0.000202	302.8	**5.331**	0.039
RMD1-328	887	328.00	0.0675	0.001588	42.5	**5.728**	0.069
*RMD1 157.4***	*926*	*368.00*	*0.0860*	*0.003029*	*28.4*	***7.225***	*0.084*
RMD1-386	925	386.00	0.0805	0.001638	49.2	**6.875**	0.093
RMD1-445	894	445.00	0.0840	0.000964	87.1	**7.331**	0.072
*RMD1 136.7***	*1055*	*462.00*	*0.0763*	*0.000571*	*133.6*	***6.622***	*0.059*
RMD1 173.3	559	467.00	0.0924	0.002521	36.7	**7.931**	0.093
RMD1 107.1	437	478.00	0.0925	0.003852	24.0	**7.977**	0.114
RMD1-497	915	497.00	0.0939	0.001651	56.9	**8.101**	0.086
RMD1 M5.6	490	523.00	0.1107	0.010362	10.7	**8.824**	0.298
RMD1-530	573	530.00	0.1026	0.002437	42.1	**8.838**	0.151
RMD1-C	600	557.00	0.1067	0.001974	54.0	**9.202**	0.140

*Excluded from model because the large associated uncertainty

** Excluded from model because outliers

Table S1

RMD1						RMD8				
Sample	z	ChRM				Sample	z	ChRM		
	mm	D (°)	I (°)	MAD (°)	D_{corr} (°)		mm	D (°)	I (°)	MAD (°)
Top	2.5					RM1	1.5	348.5	57.0	7.0
sp5	6.0					RM2	5.5	331.3	67.8	11.5
sp8	9.0	126.7	71.2	4.2	340.6	RM3	9.5	329.9	70.8	10.6
sp11	12.5	100.6	62.1	17.5	314.5	RM4	13.5	342.6	66.9	3.2
sp15	16.5	130.3	60.6	9.7	344.2	RM5	17.5	350.5	59.0	8.8
sp19	20.5	95.3	71.9	3.4	309.2	RM6	21.5	349.9	62.5	2.5
sp23	24.5	143.7	79.0	5.7	357.6	RM7	25.3	334.2	65.2	3.5
sp27	28.5	164.7	79.2	6.6	18.6	RM8	29.0	332.2	69.3	3.0
sp31	32.5	158.0	81.2	3.2	11.9	RM9	33.0	343.4	72.8	4.2
sp35	36.5	111.6	63.1	2.1	325.5	RM10	37.0	10.0	77.7	2.2
sp40	41.5	145.9	79.7	1.9	359.8	RM11	41.0	359.6	77.1	8.3
sp44	45.5	155.3	80.1	2.1	9.2	RM12	45.0	2.0	78.8	6.1
sp48	49.5	144.2	77.3	3.3	358.1	RM13	49.0	348.9	76.3	2.5
sp52	53.5	139.1	71.5	1.3	353.0	RM14	53.0	326.7	69.5	2.0
sp56	57.5	153.8	66.1	2.4	7.7	RM15	57.0	342.2	71.7	4.8
sp60	61.5	129.4	74.1	3.4	343.3	RM16	61.0	8.7	62.8	4.9
sp64	65.5	140.5	64.5	12.4	354.4	RM17	65.0	344.1	65.9	3.1
sp68	69.5	151.5	75.7	4.2	5.4	RM18	69.0	345.5	67.0	3.4
sp72	73.5	139.6	72.6	2.2	353.5	RM19	73.0	339.2	59.6	1.6
sp76	77.5	141.9	73.5	2.3	355.8	RM20	76.8	342.3	61.7	1.2
sp80	81.5	131.5	65.7	3.4	345.4	RM21	82.5	346.2	59.3	4.2
sp84	85.5	139.9	76.7	2.6	353.8	RM22	86.5	338.9	59.9	2.2

sp88	89.5	120.3	76.9	5.2	334.2	RM23	90.5	345.8	60.0	1.8
sp92	93.5	128.7	66.7	3.8	342.6	RM24	94.5	358.1	58.7	1.7
sp96	97.5	128.1	76.6	4.0	342.0	RM25	98.5	348.6	63.2	2.3
sp100	101.5	124.3	73.7	4.7	338.2	RM26	102.5	356.9	62.0	3.6
sp104	105.5	169.9	77.5	6.6	23.8	RM27	106.5	354.1	67.9	3.5
sp108	109.5	151.3	68.8	1.7	5.2	RM28	110.5	342.5	70.0	4.7
sp112	113.5	151.3	70.3	1.5	5.2	RM29	114.3	359.9	70.1	1.7
sp116	117.5	151.4	71.3	2.9	5.3	RM30	118.0	2.9	63.8	2.3
sp120	121.5	163.0	79.3	4.1	16.9	RM31	121.8	345.4	66.6	6.7
sp124	125.5	162.9	72.6	3.8	16.8	RM32	125.5	347.8	67.6	6.1
sp128	129.5	159.2	68.3	5.5	13.1	RM33	129.5	354.8	68.3	3.3
sp132	133.5	159.1	74.7	1.2	13.0	RM34	133.5	353.0	70.4	3.6
sp136	137.5	162.7	72.1	2.1	16.6	RM35	137.5	348.4	69.3	1.4
sp140	141.5	177.8	72.1	2.1	31.7	RM36	141.5	340.2	73.0	1.4
sp144	145.5	171.9	67.4	0.6	25.8	RM37	145.5	353.4	76.0	0.9
sp148	149.5	189.8	59.6	4.5	43.7	RM38	149.3	21.1	73.5	2.4
sp152	153.5	188.2	62.4	2.9	42.1	RM39	152.5	307.7	71.1	14.3
sp156	157.5	182.8	58.7	4.5	36.7	RM40	155.8	0.9	80.5	2.5
sp160	161.5	167.4	63.5	5.2	21.3	RM41	161.5	359.2	81.5	3.9
sp164	165.5	186.9	62.4	4.3	40.8	RM42	165.5	22.9	80.1	2.1
sp168	169.5	189.0	60.4	1.6	42.9	RM43	169.5	2.1	86.2	3.1
sp172	173.5	168.7	33.3	4.7	22.6	RM44	173.3	14.7	79.7	3.2
sp176	177.5	181.3	62.4	8.7	35.2	RM45	176.8	11.7	78.0	1.7
sp180	181.5	198.7	66.8	16.8	52.6	RM46	180.5	23.9	73.7	2.4
sp184	185.5	179.9	53.4	17.8	33.8	RM47	184.5	326.0	84.4	6.6
sp188	189.5	189.5	43.0	20.5	43.4	RM48	188.5	347.9	80.9	7.1
sp192	193.5	184.2	56.1	9.8	38.1	RM49	192.5	3.0	75.3	4.0
sp196	197.5	175.6	68.1	7.1	29.5	RM50	196.5	12.6	71.0	3.1

sp200	201.5	166.7	71.5	5.0	20.6		RM51	200.5	13.5	74.8	5.4
sp204	205.5	163.6	67.6	8.9	17.5		RM52	204.5	0.3	73.5	3.4
sp208	209.5	138.9	74.5	6.0	352.8		RM53	208.3	6.1	76.1	1.6
sp212	213.5	147.3	71.9	2.4	1.2		RM54	212.0			
sp216	217.5	101.5	73.7	2.9	315.4		RM55	216.0	354.8	67.1	5.5
sp220	221.5	126.2	72.6	7.5	340.1		RM56	220.0	16.0	73.4	2.7
sp224	225.5	147.3	56.4	2.1	1.2		RM57	224.0	12.2	66.5	4.4
sp228	229.5	110.6	66.4	11.4	324.5		RM58	228.0	346.8	55.6	4.1
sp232	233.5	116.4	52.7	14.3	330.3		RM59	232.0	0.4	56.6	3.3
sp236	237.5	101.3	64.5	5.1	315.2		RM60	235.5	1.7	42.2	7.5
sp240	241.5	106.5	67.0	7.3	320.4		RM61	240.0	4.5	36.6	12.1
sp244	245.5	108.1	70.2	4.8	322.0		RM62	243.5	345.7	55.8	5.9
sp248	249.5	112.8	70.1	2.7	326.7		RM63	249.5	355.9	55.7	9.7
sp252	253.5	133.3	67.4	2.5	347.2		RM64a	253.5	344.8	48.8	6.7
sp256	257.5	151.6	72.2	2.2	5.5		RM65	257.5	355.3	56.9	1.4
sp260	261.5	141.7	73.6	2.4	355.6		RM66	261.5	348.3	64.9	4.5
sp264	265.5	142.0	71.4	2.8	355.9		RM67	265.5	355.7	62.4	2.5
sp268	269.5	138.2	74.7	3.3	352.1		RM68	269.5	350.0	60.9	3.1
sp272	273.5	137.1	70.9	1.9	351.0		RM69	273.3	347.2	60.6	1.9
sp276	277.5	139.4	65.8	2.1	353.3		RM70	277.0	352.1	62.8	1.7
sp279	280.5	140.5	65.3	1.5	354.4		RM71	280.8	341.7	60.0	1.5
sp283	284.5	131.2	59.2	3.7	345.1		RM72	284.3	342.1	57.4	1.4
sp287	288.5	121.0	58.8	4.5	334.9		RM73	287.8	345.8	55.7	1.4
sp291	292.5	136.3	59.4	1.0	350.2		RM74	291.0	346.1	50.8	5.5
sp298	299.5	113.0	73.1	6.6	326.9		RM75	294.3	358.1	46.6	1.9
sp302	303.5	135.5	73.1	4.8	349.4		RM76	297.3	347.3	45.5	2.3
sp306	307.5	136.6	63.9	5.4	350.5		RM77	300.5	355.1	50.3	1.4
sp310	311.5	132.4	68.8	8.7	346.3		RM78	303.0	319.8	59.8	5.2

sp314	315.5	144.7	67.4	3.2	358.6	RM79	306.0	310.9	56.2	10.1
sp318	319.5	143.0	66.2	4.7	356.9	RM80	309.5	337.1	53.0	10.3
sp322	323.5	140.0	74.7	7.2	353.9	RM81	328.3			
sp326	327.5	139.3	66.6	4.8	353.2	RM82	332.3	350.8	75.2	2.8
sp330	331.5	126.0	64.4	3.0	339.9	RM83	336.5	346.3	72.8	2.9
sp334	335.5	140.8	67.5	2.5	354.7	RM84	339.5	354.1	77.5	2.7
sp338	339.5	132.2	56.0	1.6	346.1	RM85	343.5	352.1	72.1	8.7
sp342	343.5	134.1	65.0	2.2	348.0	RM86	347.5	355.2	69.4	2.3
sp346	347.5	125.1	55.1	2.7	339.0	RM87	351.8	351.4	66.0	3.0
sp350	351.5	132.4	52.4	2.1	346.3	RM88	355.5			
sp354	355.5	143.3	51.1	3.9	357.2	RM89	359.0	359.7	57.1	2.7
sp358	359.5	146.6	56.1	7.9	0.5	RM90	362.5	1.3	58.0	2.3
sp362	363.5	145.8	39.5	6.3	359.7	RM91	366.0	8.4	56.8	2.0
sp366	367.5	158.1	64.1	14.7	12.0	RM92	370.0	7.3	56.3	1.6
sp370	371.5	144.2	49.7	3.7	358.1	RM93	374.0	8.1	59.6	2.8
sp374	375.5	144.7	40.1	5.6	358.6	RM94	377.8	9.9	60.2	10.5
sp378	379.5	143.5	53.1	3.9	357.4	RM95	381.5	38.2	57.3	3.9
sp381	382.5	141.9	45.6	2.3	355.8	RM96	393.5	17.6	58.7	2.1
sp385	386.5	135.8	45.5	2.4	349.7	RM97	397.5	19.3	62.1	3.0
sp389	390.5	142.0	51.3	2.6	355.9	RM98	401.5	25.6	63.8	3.8
sp393	394.5	146.9	48.7	2.4	0.8	RM99	405.5	39.0	44.0	2.6
sp397	398.5	147.0	46.2	5.0	0.9	RM100	409.5	28.7	58.4	1.9
sp401	402.3	145.2	53.7	4.9	359.1	RM101	413.5	22.2	63.2	5.5
sp404.5	406.3	147.5	54.3	1.2	1.4	RM102	417.5	19.9	61.0	2.6
sp409	410.5	157.3	60.0	2.6	11.2	RM103	421.0	13.8	58.9	4.2
sp413	414.5	149.7	53.8	2.6	3.6	RM104	424.5	15.7	57.7	4.2
sp417	418.5	150.2	57.3	3.0	4.1	RM105	428.5	16.6	60.5	10.1
sp421	422.5	148.4	59.2	3.3	2.3	RM106	432.5	14.4	65.9	4.5

sp425	426.5	138.8	63.4	2.5	352.7	RM107	436.5	14.6	64.0	1.7
sp429	430.5	145.4	65.7	4.2	359.3	RM108	440.3	1.4	66.1	1.9
sp433	434.5					RM109	445.0	13.0	65.2	3.3
sp437	438.5	153.3	56.0	1.8	7.2	RM110	449.0	356.5	62.3	2.6
sp441	442.5	155.6	54.1	2.0	9.5	RM111	453.0	15.5	67.6	2.7
sp445	446.5	142.3	60.6	5.2	356.2	RM112	457.0	20.3	65.0	2.0
sp449	450.5	146.5	57.4	2.2	0.4	RM113	461.0	17.7	66.2	1.2
sp453	454.5	144.7	61.7	2.1	358.6	RM114	465.0	18.2	63.1	2.7
sp457	458.3	137.3	60.1	1.8	351.2	RM115	469.0	0.5	63.7	3.1
sp460.5	463.0	137.4	64.5	1.5	351.3	RM116	472.8	33.2	62.1	2.5
sp470.5	472.0					RM117	476.5	9.0	63.4	3.0
sp474.5	475.5	147.8	61.1	2.7	1.7	RM118	480.3	8.1	68.8	2.9
sp477.5	479.0	155.4	61.0	1.6	9.3	RM119	484.0	4.6	68.4	1.4
sp481.5	483.0	155.7	64.7	0.9	9.6	RM120	488.0	358.4	70.7	3.6
sp485.5	487.0	155.0	66.7	2.6	8.9	RM121	492.0	11.5	68.1	1.0
sp489.5	491.0	146.8	68.8	2.1	0.7	RM122	496.0	8.7	70.7	0.9
sp494.5	496.0	154.8	64.9	1.9	8.7	RM123	500.0	14.1	73.0	1.2
sp498.5	500.0	153.6	64.4	1.4	7.5	RM124	504.0	4.0	73.4	1.8
sp502.5	504.0	154.2	65.7	1.0	8.1	RM125	508.0	3.3	74.8	1.5
sp506.5	508.0					RM126	512.0	5.5	69.1	1.8
sp510.5	512.0	154.9	63.5	2.8	8.8	RM127	516.0	26.1	70.8	1.0
sp513.5	514.5	158.1	63.7	2.6	12.0	RM128	519.5	17.9	70.7	1.4
sp517.5	519.0	149.5	65.2	1.9	3.4	RM129	523.0	8.8	67.9	1.2
sp521.5	523.0	160.6	63.1	1.9	14.5	RM130	526.8	19.6	67.8	2.2
sp525.5	527.0	164.2	61.4	3.7	18.1	RM131	530.5	29.7	68.7	1.4
sp529.5	531.0	167.9	61.1	0.8	21.8	RM132	534.5	15.9	66.7	1.4
sp533.5	535.0	151.3	59.2	1.6	5.2	RM133	539.5	20.3	65.1	1.2
sp537.5	539.0	133.8	69.7	2.4	347.7	RM134	543.5	6.1	66.0	1.4

sp541.5	543.0	146.2	66.3	2.9	0.1	RM135	547.5	4.0	63.1	1.4
sp544.5	545.5					RM136	551.5	28.7	49.4	1.6
sp548.5	550.0	151.9	69.1	4.1	5.8	RM137	555.5	5.9	62.9	2.2
sp552.5	554.0	150.6	61.0	2.0	4.5	RM138	559.3	349.7	50.7	3.7
sp556.5	558.0	128.6	52.6	2.0	342.5	RM139	563.0	31.6	41.8	1.7
sp564.5	566.0	118.9	50.9	1.4	332.8	RM140	567.0	10.4	45.9	1.0
sp568.5	570.0	125.2	48.9	4.2	339.1	RM141	571.0	12.2	42.7	1.9
sp580	581.5					RM142	575.0	22.5	47.6	6.1
sp584	585.5	133.3	41.8	5.9	347.2	RM143	579.0	9.0	29.4	9.4
sp588	589.0	152.6	41.0	6.6	6.5					
sp591	592.0	145.4	54.8	4.3	359.3					

Table S2